

# The effect of normal load on polytetrafluoroethylene tribology

Peter R Barry<sup>1</sup>, Patrick Y Chiu<sup>1</sup>, Scott S Perry<sup>1</sup>,  
W Gregory Sawyer<sup>1,2</sup>, Simon R Phillpot<sup>1</sup> and Susan B Sinnott<sup>1,3</sup>

<sup>1</sup> Department of Materials Science and Engineering, University of Florida, Gainesville, FL 32611-6400, USA

<sup>2</sup> Department of Mechanical and Aerospace Engineering, University of Florida, Gainesville, FL 32611-6250, USA

E-mail: [sinnott@mse.ufl.edu](mailto:sinnott@mse.ufl.edu)

Received 27 July 2008, in final form 7 October 2008

Published 18 March 2009

Online at [stacks.iop.org/JPhysCM/21/144201](http://stacks.iop.org/JPhysCM/21/144201)

## Abstract

The tribological behavior of oriented poly(tetrafluoroethylene) (PTFE) sliding surfaces is examined as a function of sliding direction and applied normal load in classical molecular dynamics (MD) simulations. The forces are calculated with the second-generation reactive empirical bond-order potential for short-range interactions, and with a Lennard-Jones potential for long-range interactions. The range of applied normal loads considered is 5–30 nN. The displacement of interfacial atoms from their initial positions during sliding is found to vary by a factor of seven, depending on the relative orientation of the sliding chains. However, within each sliding configuration the magnitude of the interfacial atomic displacements exhibits little dependence on load over the range considered. The predicted friction coefficients are also found to vary with chain orientation and are in excellent quantitative agreement with experimental measurements.

(Some figures in this article are in colour only in the electronic version)

## 1. Introduction

Poly(tetrafluoroethylene) (PTFE) is known to have a low friction coefficient [1–3] and has been used in applications ranging from low friction bearings to nonstick frying pan coatings. It is also known for its excessively high wear rates compared to many common bulk polymers [4]. Consequently there is a concerted effort to design composites [5–7] that enhance the wear properties of PTFE while maintaining its low friction.

A key tool in the collective effort to clarify the origins of friction is atomic-level simulation, which has the ability to provide insight into potential atomic-level mechanisms that may be correlated to macroscopic friction phenomena. Many of the insights recently obtained by atomistic simulation are in good agreement, at least qualitatively, with prior experimental results [8–11]. For example, in their atomic-scale molecular dynamics friction simulations of hydrogen-terminated diamond (111) against diamond (111) surface

coated with amorphous, hydrogen-free carbon films, Gao *et al* [12] predicted similar friction forces for different amorphous film thickness. Their findings on the friction response due to counterface saturation by varying the hydrogen terminations of interfacial carbons are in good qualitative agreement with what is known about diamond-like carbon films [13]. A more recent study by Jang *et al* [14] reported on the atomic-level mechanisms associated with friction at PTFE surfaces as a function of sliding direction relative to chain orientation. The combination of simulation predictions and experimental data that spanned length scales from nanometers to centimeters and timescales from nanoseconds to seconds provided a consistent, atomic-level depiction of how the structural anisotropy of aligned PTFE contributes to its tribological properties. In particular, it was found that the sliding of oriented chains parallel to the chain backbone in both PTFE surfaces results in both low friction and low barriers to interfacial slip, whereas the sliding of oriented chains perpendicular to the chain backbone resulted in high friction and excessive molecular displacement via a plowing mechanism.

<sup>3</sup> Author to whom any correspondence should be addressed.

Here, PTFE surfaces with oriented chains are slid against one another in the parallel and perpendicular directions over a range of normal loads. The objective is to elucidate the effect of PTFE–PTFE surface loading on the aforementioned frictional anisotropy and to subsequently make a quantitative comparison to experimental results.

## 2. Methods

Classical molecular dynamics (MD) simulations [15, 16] are used in which Newton's equations of motions are numerically integrated with a third-order Nordsieck predictor corrector. The short-ranged forces are calculated using the many-body, second-generation reactive empirical bond-order potential [17], with a cutoff of 0.2 nm for C–C interactions. The long-ranged van der Waals forces are calculated using standard Lennard-Jones (LJ) potentials [16] with a cutoff of 0.57–0.84 nm; the time step is 0.2 fs.

In its solid state, PTFE exists in four main conformations, three of which are helical while the fourth is a planar zigzag, non-helical phase III which occurs under hydrostatic pressure conditions on the order of 600 MPa [18]. In these simulations, the non-helical phase III is equilibrated with the combined short and long-ranged potentials mentioned above in order to approximate the polymer's helical structure. Although electrostatic interactions play a prominent role in modeling the various helical conformations of fluoropolymers [19, 20], the effect of these interactions are somewhat diminished by the high contact pressures explored in our simulations. Our van der Waals treatment of these long-range forces may slightly underestimate the true interactions; however, they should give a reasonable description of the non-bonded intermolecular interactions.

The MD simulations are carried out with a constant number of atoms, temperature and simulation cell size where the dimensions of the PTFE surfaces are allowed to change within the confines of the fixed simulation cell size. Periodic boundary conditions [16] are applied in two directions to remove edge effects in the sliding surfaces and to more closely mimic real systems. Each PTFE surface contains seven layers of chains for a total thickness of 4.0 nm and a sliding surface area of  $4.5 \text{ nm} \times 4.5 \text{ nm}$  (see figure 1). The bottom layer of the lower film is fixed and the top layer of the upper surface moves as a rigid unit to compress and slide the top surface against the bottom surface. The forces on the top surface are recorded and analyzed.

In order to maintain the temperature of each surface at 298 K and also to mimic the thermal dissipation which occurs in experimental samples, Langevin frictional and stochastic forces [16] are applied to the two layers of chains closest to the fixed or rigid moving regions of both the upper and lower PTFE films in the two directions normal to the direction of sliding (see figure 1). The cross-link density of each PTFE surface is approximately  $2.83 \text{ nm}^{-3}$ . A constant sliding rate of  $10 \text{ m s}^{-1}$  is employed.

Prior to sliding, both PTFE surfaces are equilibrated with a 1 nm gap between them until the system energy fluctuates in a narrow energy band around a constant value. The top surface

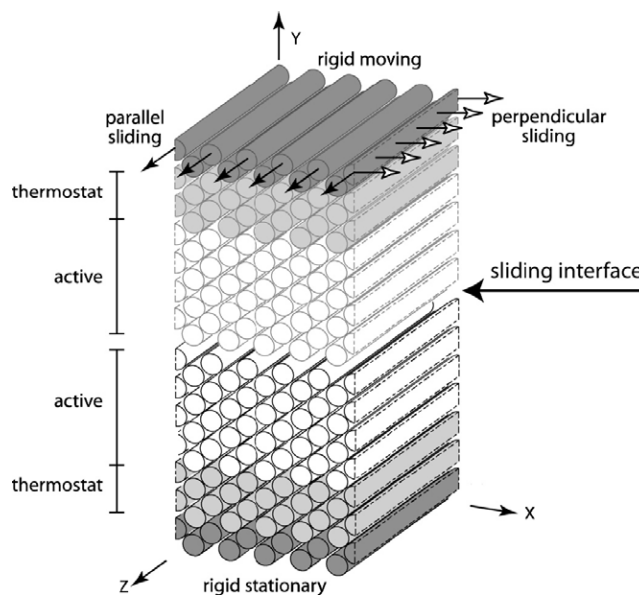


**Figure 1.** Schematic of the system used in the MD simulations. The system is periodic along the  $x$  and  $z$  directions, which make up the surface plane. The simulation cell is comprised of two cross-linked, aligned PTFE surfaces. Each PTFE surface consists of regions of rigid atoms, thermostated atoms, and active atoms of layer thickness 0.6, 1.2 and 2.2 nm respectively. After equilibration, the lower surface is held stationary while the upper block of rigid atoms in the upper surface is moved in the  $z$  direction (parallel) or the  $x$  direction (perpendicular), where parallel and perpendicular refer to the sliding direction relative to the chain alignment, as indicated.

is then incrementally compressed and equilibrated against the bottom surface to establish a distinct contact pressure within a narrow range. Upon achieving the target contact pressure, the two films are further equilibrated to minimize the forces between the compressed polymer chains. To perform the tribological simulation, the top film is then slid unidirectionally for  $\sim 36 \text{ nm}$  against the stationary lower film. The sliding is done either parallel (i.e., parallel sliding) or perpendicular (i.e., perpendicular sliding) to the axes of the aligned PTFE chains in both surfaces (figure 1). The evolution of the predicted frictional and normal forces for each established contact pressure is then recorded. These values are used to quantitatively determine the friction coefficients and adhesive force for the system for both sliding configurations. In particular, a Monte Carlo method is used to determine the friction coefficient from the force data, as described in the appendix. While the simulations are carried out at constant interfacial displacement, the contact pressures explored in the simulations are high, are taken over a broad range, and are on the order of those found in actual tribological contacts.

## 3. Results and discussion

Compared to the earlier analysis of Jang *et al* [14], the results reported here are a more accurate prediction of the friction coefficient of aligned PTFE. This is achieved by plotting frictional force versus normal force, as illustrated in figure 2, and by taking a series of least-squares fits to the data, the

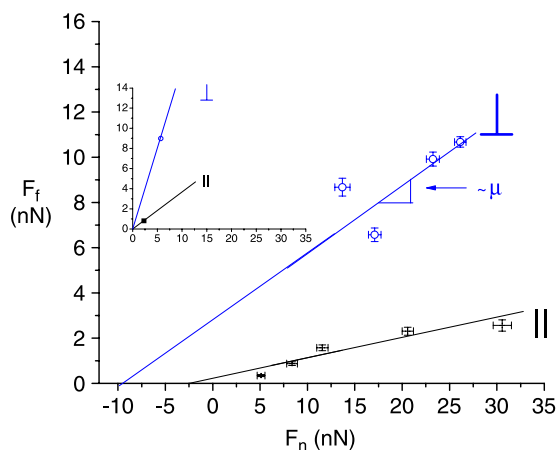


**Figure 2.** In the main graph of this figure, friction coefficients ( $\mu$ ) of 0.28 and 0.09 were obtained using boxcars corresponding to 0.2 nm of sliding fit to the respective data points for perpendicular and parallel sliding configurations, respectively. Adhesive forces ( $F_a$ ) of 12.0 and 2.7 between the two sliding surfaces for perpendicular and parallel sliding, respectively, are also approximated by taking the corresponding average of the  $x$ -intercepts from the least-squares fits. Additional details of the procedure are given in the appendix. The inset summarizes the simulation results by Jang *et al* [14], where the friction coefficient for each sliding configuration was approximated by the slope of the line between the origin and corresponding data point. Friction coefficients of  $\sim 0.63$  and  $\sim 0.35$  for perpendicular and parallel sliding, respectively, were reported previously.

details of which are discussed in the appendix. The slopes of the least-squares fits yield the magnitudes of the friction coefficients. Friction coefficients of  $0.28 \pm 0.01$  and  $0.09 \pm 0.01$  for perpendicular and parallel sliding, respectively, are predicted. These results are in pleasing agreement with the experimental values of about 0.3 and 0.1, respectively [14, 21].

The values previously reported by Jang *et al* [14] were considerably larger. The difference arises not from any differences in the simulations themselves, but rather in their analysis. In particular, in the work of Jang *et al* the friction

coefficients were estimated from the frictional force at a single load under the assumption that the frictional force at zero load is zero, as indicated in the inset to figure 2. That is, it was assumed that there is no adhesive force during sliding, an assumption that figure 2 demonstrates to be incorrect. Despite these quantitative differences the physical reasoning and conclusions of the previous work stand.

All other things being equal, we would expect that adhesion would be proportional to the real area of contact and, in some cases, to the amount of time the two surfaces are held in continuous contact [22]. The parallel configuration yields the maximum possible real area of contact due to the uninterrupted interlocking of chains at the sliding interface during sliding. For the perpendicular sliding configuration the contact is interrupted during sliding and is further complicated by the significant amount of ensuing molecular wear. Based on the above argument, we would expect a larger adhesive force for parallel sliding than for perpendicular sliding. An extrapolation of the least-squares fit on our frictional versus normal force curves to low normal loads gives the associated adhesive contribution to friction. As figure 2 indicates, our simulations actually predict higher adhesion for the perpendicular configuration, the opposite of what we argued above. The reconciliation of this disagreement most likely lies with the changing topography of the interface in the sliding direction, which plays a significant role in the predicted adhesive force. Indeed, analysis of the coordination of the carbons atoms at the sliding interface reveals only a 1% change in coordination for the parallel sliding, but a 4% change for perpendicular configurations. While this difference in the amount of bond breaking should result in a larger adhesive force for perpendicular sliding than parallel sliding, it probably cannot explain the full difference. This suggests that the molecular wear in the form of gross chain movement (discussed in detail below) may be the predominant source of adhesion, rather than the rearrangement of atoms within the polymer chain. These issues are still not fully resolved.

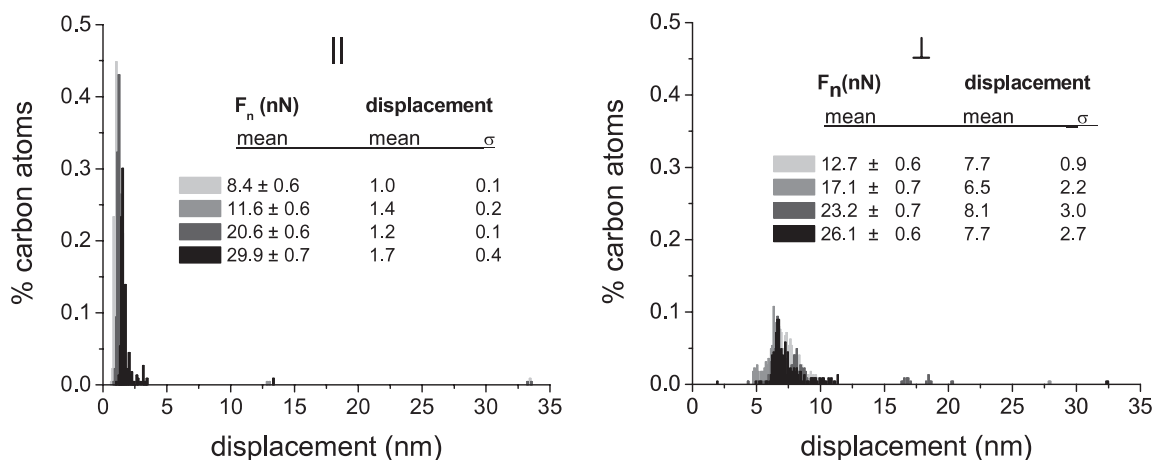


**Figure 3.** Distribution of the displacement of carbon atoms from their initial positions prior to sliding in the lower PTFE surface at the sliding interface. Significantly less interfacial atomic displacement is predicted, on average, for the parallel sliding configuration (left) compared to the perpendicular sliding (right), even at high normal loads. In each of the cases for parallel sliding, two carbon atoms (the same carbon atoms in each case) broke off from the fourth polymer chain and was displaced significantly further in the direction of sliding than the average displacement of the group as is evidenced by the very short peaks at  $\sim 13$  and 32 nm.

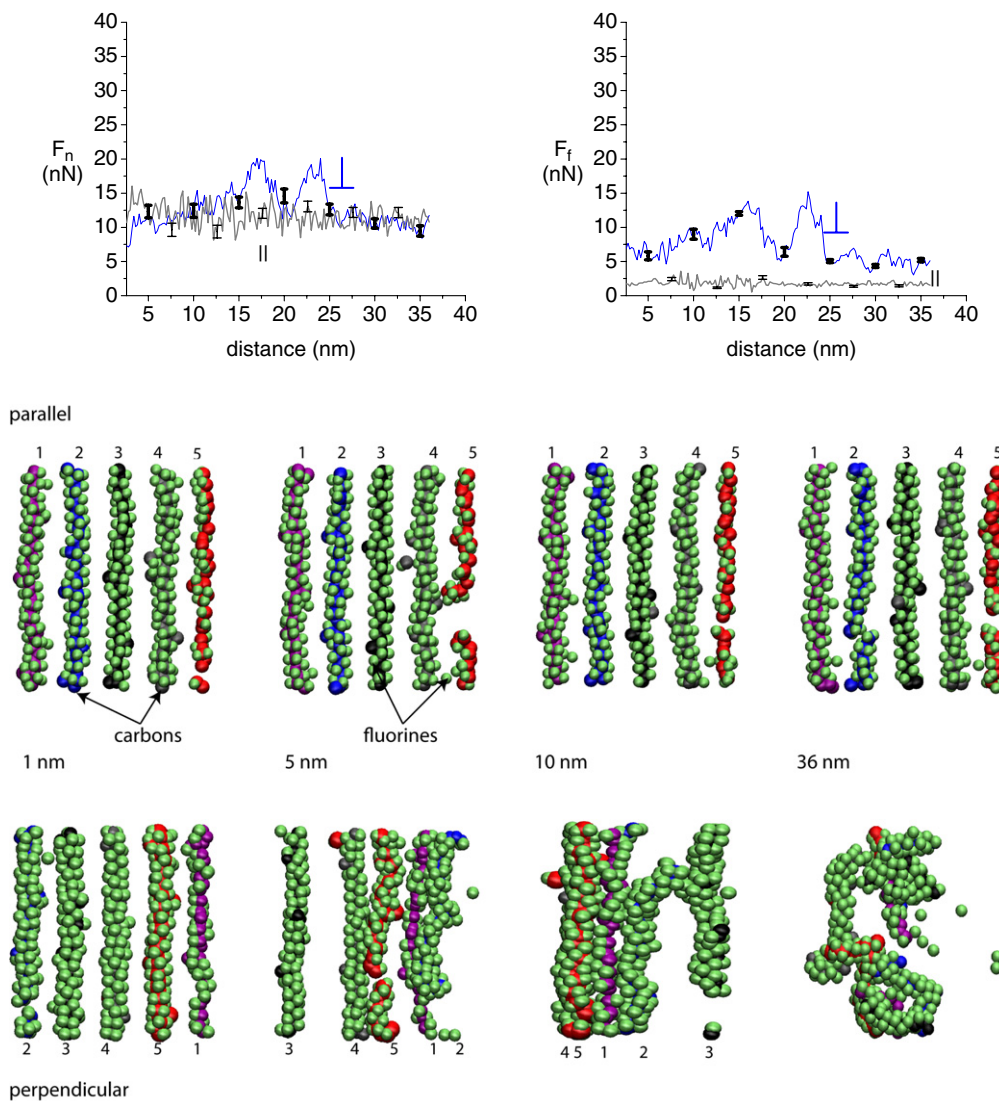


**Figure 4.** The predicted normal ( $F_n$ ) and frictional ( $F_f$ ) forces (in nN) for both parallel ( $\parallel$ ) and perpendicular ( $\perp$ ) sliding at relatively low comparable normal loads. The average values are given in table 1. Snapshots of the interface at various sliding distances are also shown. The topmost chains of the lower PTFE surface are shown where the carbon atoms in chains one through five are indicated. The sliding direction for the perpendicular configuration is from right to left and from bottom to top along the chain backbone orientation for the parallel configuration.

The strong asymmetry seen here between parallel and perpendicular sliding was seen in our earlier simulations [14, 23, 24]. The earlier work found noticeable alternations between high and low values in the evolution of both the normal and frictional forces for perpendicular sliding. Such behavior is not surprising considering the topography of the sliding interface explored in the case of perpendicular sliding, where the normal pressures are expected to be lower when the polymer chains of the upper and lower films are interdigitated and higher when the chains are directly on top of each other. The converse is expected for the frictional force. As noted in those studies, the effect is likely further enhanced by the extensive damage at the interface arising from agglomeration and subsequent breaking of the aligned chains. The opposite scenario is the case for the parallel sliding configuration where the aligned PTFE chains of the upper and lower films are initially interlocked with each other and remain in registry. Ad-

ditionally, the topography of the sliding interface explored was significantly smoother than that for the perpendicular configuration and thus resulted in smaller variations in the normal and frictional forces. As a result, significantly less wear was reported compared to the perpendicular sliding configuration.

Not surprisingly, similar behavior corresponding to those findings is found here for perpendicular and parallel sliding. Somewhat surprising however, is the minimum amount of molecular rearrangement experienced in the case of parallel sliding even at extremely high loads. To quantify the amount of molecular rearrangement due to sliding, the displacement of interfacial carbon atoms in the sliding direction of the lower surface relative to their initial positions is determined. As figure 3 indicates, for parallel sliding the average atomic displacement of  $\sim 1$  nm of these carbon atoms due to sliding at a normal load of approximately 30 nN (i.e.,  $\sim 1.5$  GPa) is statistically identical to the displacement under sliding at

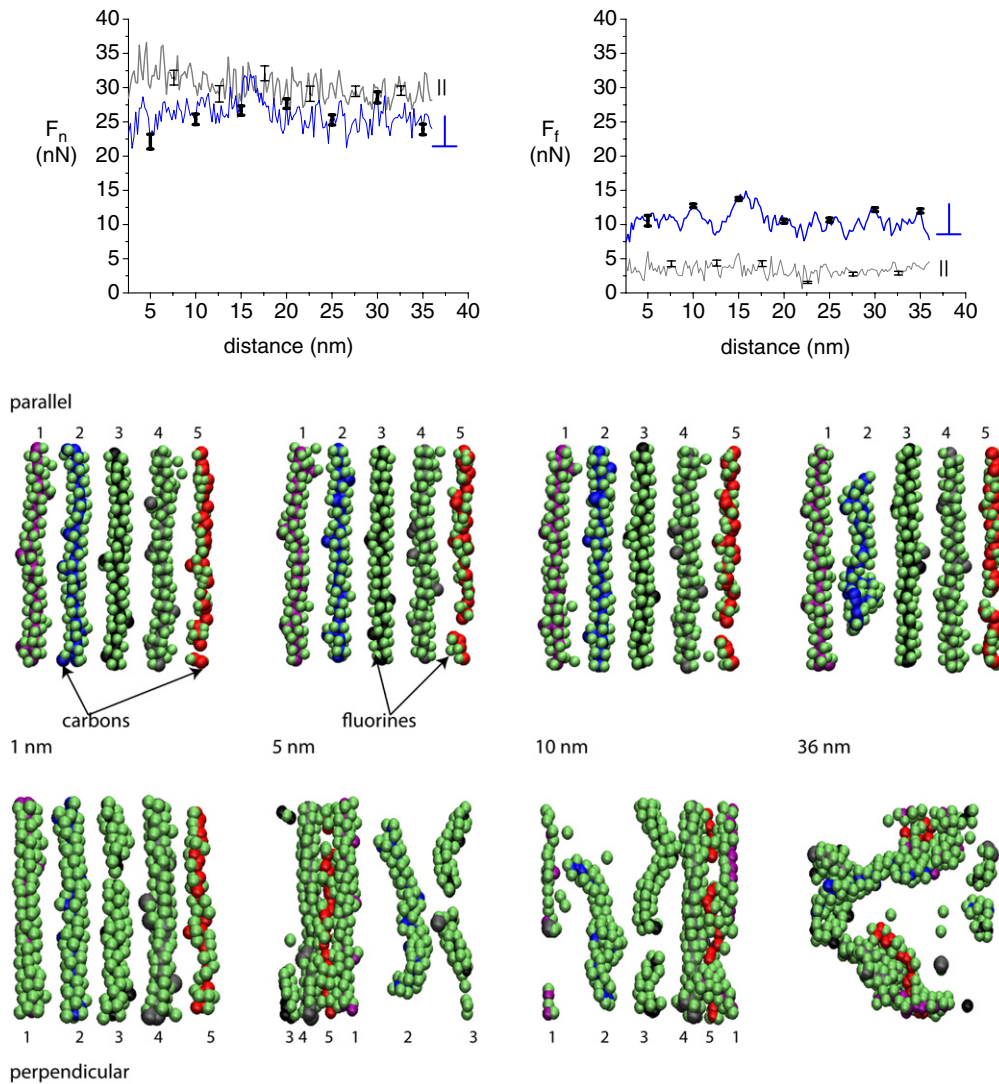


**Figure 5.** The predicted normal ( $F_n$ ) and frictional ( $F_f$ ) forces (nN) for both parallel ( $\parallel$ ) and perpendicular ( $\perp$ ) sliding at relatively high comparable normal loads. The average values are given in table 2. Snapshots of the interface at various sliding distances are also shown. The topmost chains of the lower PTFE surface are shown where the colors used are identical to those used in figure 4. The sliding direction for the perpendicular configuration is from right to left and from bottom to top along the chain backbone orientation for the parallel configuration.

a normal load of roughly 5 nN (i.e.,  $\sim 0.25$  GPa). This displacement should not be interpreted as damage to the surface, but merely as the result of the elastic deformation of the polymer as a whole. In the case of the perpendicular sliding configuration the atomic displacements are much larger ( $\sim 7$  nm), but still small compared to the overall sliding distance of  $\sim 36$  nm. Again, the results are largely load-insensitive. These larger displacements are associated with significant molecular wear.

The effect of normal load on the frictional force at relatively low and high normal loads for both the perpendicular and parallel sliding configurations is illustrated in figures 4 and 5. The numerical values of the forces shown in these figures are given in tables 1 and 2. These figures and tables reveal that for approximately equal normal forces, the frictional force for perpendicular sliding is 3–5 times larger than that for the parallel sliding configuration. Tables 1 and 2 also indicate that even when the normal forces for perpendicular sliding are roughly doubled, the frictional force increases by a

factor of 1.6. For the parallel configuration, the normal force is tripled while the frictional force increases only by a factor of  $\sim 1.8$ . Data taken for normal loads in the range of 5–30 nN reveal that the average carbon–carbon distance between the interfacial chains of the upper and lower surfaces range from approximately  $3.3 \pm 0.2$  to  $2.6 \pm 0.2$ , respectively. That is, much of the load is absorbed by an overall compression of the polymer surfaces themselves, rather than by an increase in the load at the interface. Thus there is a relatively small change in the real area of contact at the polymer–polymer interface even for large increases in load.

The molecular snapshots of the sliding interface at 1, 5, 10 and 36 nm of sliding, shown in figures 4 and 5, give a microscopic view of the structural evolution of the surface. Examining parallel sliding first (figure 4), we see that there is almost no molecular wear at the lower load. A molecular segment of chain five slips in the sliding direction at  $\sim 5$  nm but the break is almost completely healed as sliding progresses. Additionally, a segment of chain number two is slightly

**Table 1.** Average values of the predicted normal ( $F_n$ ) and frictional ( $F_f$ ) forces (in nN) for both parallel ( $\parallel$ ) and perpendicular ( $\perp$ ) sliding at relatively low comparable normal loads.

| Sliding configuration | $F_n$ (nN)     | $F_f$ (nN)    |
|-----------------------|----------------|---------------|
| Parallel              | $11.6 \pm 0.6$ | $1.6 \pm 0.1$ |
| Perpendicular         | $12.7 \pm 0.6$ | $6.9 \pm 0.3$ |

**Table 2.** Average values of the predicted normal ( $F_n$ ) and frictional ( $F_f$ ) forces (in nN) for both parallel ( $\parallel$ ) and perpendicular ( $\perp$ ) sliding at relatively high comparable normal loads.

| Sliding configuration | $F_n$ (nN)     | $F_f$ (nN)     |
|-----------------------|----------------|----------------|
| Parallel              | $29.9 \pm 0.7$ | $2.8 \pm 0.2$  |
| Perpendicular         | $26.1 \pm 0.6$ | $10.7 \pm 0.2$ |

displaced at  $\sim 36$  nm, hinting at the possible onset of slip as described previously for chain number five. At the higher load (figure 5), by contrast, observable molecular deformation occurs to one chain. The signature of this in figure 3 is the tail in the displacement distribution to  $\sim 3$  nm. By contrast, the perpendicular sliding cases show significant molecular wear at both high and low loads, with the aligned structure of the separated chains breaking down to a significant extent in both cases. After  $\sim 36$  nm of sliding, it is clear that the damaged, shorter chain fragments begin to align with the direction of sliding.

#### 4. Conclusions

The MD simulation results reported here reveal the influence of normal loads on the atomic responses while sliding oriented PTFE chains. By varying the normal load, the effect of associated adhesive forces during sliding are determined and their contribution to friction is quantified. The resulting predicted friction coefficients are in excellent quantitative agreement with experimental values. The simulations also illustrate how the relative orientation of the chains alters their molecular-scale responses at low and high normal loads. Similar to the findings of Gao *et al* [12], we believe that the structure and overall topography of the PTFE surfaces contribute significantly to the predicted behavior described herein and that the thickness of the PTFE surfaces is not expected to significantly alter the qualitative trends described over the contact pressures considered. Even though the PTFE surfaces examined in this study were cross-linked, thicker samples may provide more opportunistic slip interfaces within each of the surfaces. As a result, additional wear mechanisms may become activated at elevated pressures and temperatures; thus, potentially leading to quantitatively different friction behavior.

#### Acknowledgments

This was supported by an AFOSR-MURI grant FA9550-04-1-0367. Any opinions, findings, conclusions, or recommendations expressed in this material are those of the authors and do not necessarily reflect the views of the Air Force

Office of Scientific Research. The University of Florida High-Performance Computing Center is acknowledged for providing computational resources and support. The authors also thank R K Behera and F Foertter for valuable discussions.

#### Appendix

A single sliding simulation of 36 nm at  $10 \text{ m s}^{-1}$  with a 0.2 fs time steps with data taken every 1000 steps (equivalent to 200 fs of time and 2 pm of sliding) yields 18 000 instantaneous values for the frictional and normal forces. Here we briefly explain the process used to reduce this large data set to scientifically and statistically meaningful results. First, the large number of data points was reduced using boxcar averaging of 100 data points corresponding to 0.2 nm of simulated sliding. This distance was chosen as it is similar to the spatial resolution of microscopic tribological experiments. For the  $i$ th boxcar, the average force is  $f_i$  and the standard deviation is  $\sigma_i$ . This produces the data points shown in figures 4 and 5; the standard deviation of the mean,  $\sigma_i/\sqrt{n}$ , from these 100-point data sets was also determined.

These 0.2 nm-averaged forces and  $\sigma$  were then used for the calculation of the average forces. The quantification of the forces, give in the various tables above, were calculated using a weighted average [25]:

$$f_{\text{best}} = \frac{\sum_{i=1}^N w_i f_i}{\sum_{i=1}^N w_i}, \quad (1)$$

where  $w_i = 1/\sigma_i^2$ . The uncertainty in the weighted average force was then calculated in the standard way as

$$\sigma_{\text{best}} = \left( \sum_{i=1}^N w_i \right)^{-1/2}. \quad (2)$$

The process defined above is not unique, in that different choices of the size of the boxcars would yield slightly different final results (see table A.1). The non-uniqueness of the analysis notwithstanding, we justify the particular choice of the size of the boxcars as being representative of the spatial resolution achievable in experiment.

The first 2.4 nm of sliding was omitted from the calculation of all averages so as to exclude the initial elastic response of the two surface polymer system to shear stress.

For many tribological situations, the friction coefficient  $\mu$  is defined as  $\mu = F_f/F_n$  where  $F_f$  is the frictional or lateral force and  $F_n$  is the normal force. In this work, simulations were carried out such that the different frictional forces were determined for a number of different normal loads; similar normal loads were used for perpendicular and parallel sliding. The related uncertainties for each  $F_f$  and  $F_n$  were calculated as described above.

A Monte Carlo method was used to determine the friction coefficient from the force data. In particular, for each of the ( $F_f, \sigma_f$ ) and ( $F_n, \sigma_n$ ) pairs, approximately 2000 statistical justifiable possible friction and normal forces were generated in Microsoft Excel using a one-dimensional random walk where the  $(n + 1)$ st value for  $F_f$  is determined from the  $n$ th

**Table A.1.** Variation in the quantification of the forces from different boxcar averages. The frictional and normal forces for the parallel configuration given in table 1 are used as examples. The values for the original, unreduced (18 000 data point) simulation set is given in the second column by simply taking the arithmetic mean of the data set. The uncertainty in the average was taken as the standard deviation of the mean [25]. The other averages are weighted and were computed from reduced data sets (see the discussion in the appendix). The table shows the spatial resolution between data points for each averaged case.

| Size of boxcar average | 1<br>(original data) | 10                         | 50             | 100            | 500            | 1000           |
|------------------------|----------------------|----------------------------|----------------|----------------|----------------|----------------|
| Distance (nm)          | 0.002                | 0.02                       | 0.1            | 0.2            | 1              | 2              |
| $F_n$                  | $13.8 \pm 0.06$      | $9.6 \pm 0.1$              | $11.7 \pm 0.4$ | $11.6 \pm 0.6$ | $11.8 \pm 1.3$ | $11.8 \pm 1.9$ |
| $F_f$                  | $1.6 \pm 0.02$       | $(6 \pm 6) \times 10^{-5}$ | $0.4 \pm 0.04$ | $1.6 \pm 0.3$  | $1.7 \pm 0.3$  | $1.8 \pm 0.4$  |

**Table A.2.** A comparison of the calculated friction coefficients and adhesive force obtained using the Monte Carlo method described in the appendix. The averages of the MD force data ( $F_f$  and  $F_n$ ) obtained in this manner ('reduced' case) are compared to the results from a simple average of the original data ('unreduced' case).

|       | Perpendicular<br>reduced | Perpendicular<br>unreduced | Parallel<br>reduced | Parallel<br>unreduced |
|-------|--------------------------|----------------------------|---------------------|-----------------------|
| $\mu$ | 0.28                     | 0.28                       | 0.09                | 0.09                  |
| $F_a$ | 12.0                     | 12.0                       | 2.8                 | 8.1                   |

value according to  $F_f(n + 1) = F_f(n) + \alpha \sigma_f$ , where  $\alpha$  is a random number between  $-0.5$  and  $5$ . This process leads to a statistically normal distribution in  $F_f$  as is illustrated in figure A.1. A least-squares fit was then calculated for each set of new data ( $F_f(n)$  and  $F_n(n)$  and their uncertainties) generated. The average slope of these least-square fits were taking as our best prediction of the friction coefficient. The standard deviation of the mean was taken as the uncertainty in the measurement.

Figure A.1 illustrates a few examples of the least-square fits calculated from the generated data. Calculation of friction coefficients in this manner also allows for the determination of the adhesive contribution to sliding friction which is the value of the  $x$ -intercept of the least-squares fits. As in the case of the coefficient of friction, the average of the  $x$ -intercepts of the least-square fits and the corresponding standard deviations of the mean were taken as the best approximation of the adhesive force and uncertainty, respectively.

This approach to determine the friction coefficient and adhesive forces yields results that are almost identical to that obtained from the original, unreduced data set for  $F_f$  and  $F_n$ . Averages for  $F_f$  and  $F_n$  for the original data set were computed by taking the arithmetic mean of the data sets. The uncertainties for each mean are given as the standard deviation of the mean. Table A.2 gives numerical values for friction coefficient and adhesive force based on reduced and unreduced force averages. The numerical values obtained were identical except for the adhesive force for the parallel sliding configuration, which is accounted for by the fact that the  $y$ -intercepts of the least-square fits are between 1 and 0. As a result, small variations in this value lead to what appears to be significant changes in the  $x$ -intercepts that correspond to the adhesive force. The uncertainties in  $\mu$  and  $F_a$ , determined from the standard deviation of the mean and the propagation of uncertainties [25], are not shown since the values are significantly smaller than the calculated averages.

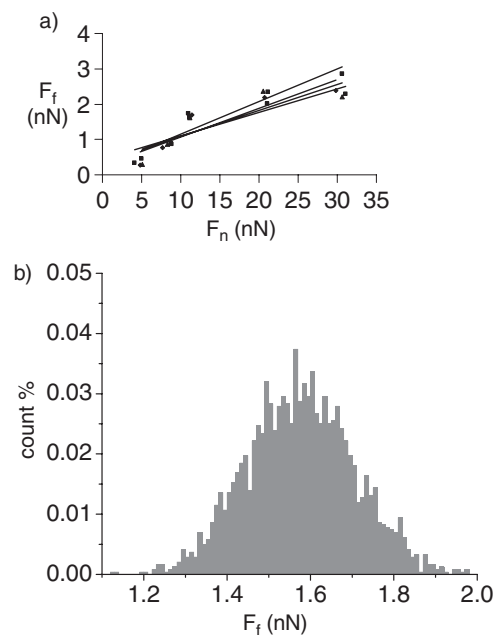


**Figure A.1.** (a) Graphical illustration of the series of least-squares fits to the randomly generated frictional and normal forces. The averages of the slopes and corresponding  $x$ -intercepts were taking as the best approximation of the friction coefficient and adhesive force respectively. The graph illustrates a small portion of the data for the parallel sliding configuration. (b) A typical example distribution of generated force data. In this example, the graph corresponds to the  $F_f$  for parallel sliding given in table 1.

## References

- [1] Pooley C M and Tabor D 1972 *Proc. R. Soc. A* **329** 251
- [2] Pooley C M and Tabor D 1972 *Nature* **237** 88
- [3] Burris D L, Perry S S and Sawyer W G 2007 *Tribol. Lett.* **27** 323
- [4] Moore D F 1975 *Principles and Applications of Tribology* (Oxford: Pergamon) p 388
- [5] Bahadur S and Tabor D 1984 *Wear* **98** 1
- [6] Blanchet T A and Kennedy F E 1992 *Wear* **153** 229
- [7] Burris D L and Sawyer W G 2006 *Wear* **260** 915
- [8] Ni B and Sinnott S B 2001 *Surf. Sci.* **487** 87
- [9] Dickrell P L, Pal S K, Bourne G R, Muratore C, Voevodin A A, Ajayan P M, Schadler L S and Sawyer W G 2006 *Tribol. Lett.* **24** 85
- [10] Harrison J A, Stuart S J and Brenner D W 1999 *Handbook of Micro/Nanotribology* ed B Bhushan (Boca Raton, FL: CRC Press) p 525
- [11] Liley M, Gourdon D, Stamou D, Meseth U, Fischer T M, Lautz C, Stahlberg H, Vogel H, Bernham N A and Duschl C 1998 *Science* **280** 273

- [12] Gao G T, Mikulski P T and Harrison J A 2002 *J. Am. Chem. Soc.* **124** 7202
- [13] Erdemir A and Donnet C 2001 Tribology of diamond, diamond-like carbon and related films *Modern Tribology Handbook* (Boca Raton, FL: CRC Press) p 871
- [14] Jang I, Burris D L, Dickrell P L, Barry P R, Santos C, Perry S S, Phillpot S R, Sinnott S S and Sawyer W G 2007 *J. Appl. Phys.* **102** 123509
- [15] Fenkel D and Smit B 2002 *Understanding Molecular Simulations from Algorithms to Applications* (San Diego, CA: Academic) p 638
- [16] Allen M P and Tildesley D J 1987 *Computer Simulation of Liquids* (Oxford: Clarendon) p 385
- [17] Brenner D W, Shenderova O A, Harrison J A, Stewart S J, Ni B and Sinnott S B 2002 *J. Phys.: Condens. Matter* **14** 783
- [18] Flack H D 1972 *J. Polym. Sci. A2* **10** 1799
- [19] Holt D B, Farmer B L, Macturk K S and Eby R K 1996 *Polymer* **37** 1847
- [20] Jang S S, Blanco M, Goddard W A, Caldwell G and Ross R B 2003 *Macromolecules* **36** 5331
- [21] McCook N L, Burris D L, Dickrell P L and Sawyer W G 2005 *Tribol. Lett.* **20** 109
- [22] Bhushan B 2002 *Introduction to Tribology* (New York: Wiley) p 732
- [23] Heo S, Jang I, Barry P R, Phillpot S R, Perry S S, Sawyer W G and Sinnott S B 2008 *J. Appl. Phys.* **103** 083502
- [24] Barry P R, Jang I, Perry S S, Sawyer W G, Sinnott S B and Phillpot S R 2007 *J. Comput.-Aided Mater. Design* **14** 239
- [25] Taylor J R 1997 *An Introduction to Error Analysis: the Study of Uncertainties in Physical Measurements* (Sausalito: University Science Books) p 270